Lightweight Tissue Tonometer Device for Detecting Pitting Edema

Jago Dorn[1,2] (jpd101) Lauren Hong[1] (syh26) Connor Kissack[1] (cak173) Jhosua Oajaca[1,2] (jao101)

Technical Advisor: Dr. Zonghe Chua, Assistant Professor, Department of Electrical, Computer, and Systems Engineering, Case School of Engineering

Instructor: Dr. Vira Chankong

Submitted for ECSE 398 in partial fulfillment for the degree of Bachelor of Science of

Electrical Engineering[1] | Systems & Control Engineering[2]

Case Western Reserve University

Fall 2025

Academic Integrity Policy

All students in this course are expected to adhere to the University standards of academic integrity. Cheating, plagiarism, misrepresentation, and other forms of academic dishonesty will not be tolerated. This includes, but is not limited to, consulting with another person during an exam, turning in written work that was prepared by someone other than you, making minor modifications to the work of someone else and turning it in as your own, or engaging in misrepresentation in seeking a postponement or extension. Ignorance will not be accepted as an excuse. If you are not sure whether something you plan to submit would be considered either cheating or plagiarism, it is your responsibility to ask for clarification. For complete information, please go to https://students.case.edu/community/conduct/aiboard/policy.html.

The individual(s) submitting this document affirm compliance with the above statement

[This page intentionally left blank]

Executive Summary

Pitting edema is a symptom of the accumulation of intercellular fluid in tissue cells that results from an increase in interstitial fluid, characterized by swelling of tissues and formation of an indentation wherever pressure is applied to the skin. While early detection is critical because it indicates underlying heart, liver, or kidney issues, current diagnostic methods are subjective, relying solely on a clinician's visual assessment and grading of the skin indentation and rebound time. To address the lack of standardization, potential misclassification of severity, and delayed diagnosis, we designed a feedback-controlled tonometer capable of applying a known force and precisely measuring skin displacement and the normal force exerted by the skin on the device. Our methodology integrates three primary subsystems: (1) a capacitive force sensor to measure the force applied to the skin, utilizing two isolated copper plates and a capacitance-to-digital converter (FDC1004) to quantify the normal force; (2) an infrared displacement sensor (TCND5000) to measure the depth of the pit formed; and (3) a pneumatic actuator that uses a syringe pump, motor, and motor driver to regulate the pressure in a silicone bellow to apply constant indentation. We expect the device to apply a controlled force of approximately 10 N and measure skin indentation. We expect the prototype to deliver consistent, precise performance across its subsystems. The device is designed to measure internal actuation displacement over a range of 0–12 mm. Additionally, the device will record and process data sufficient to classify pitting edema into the four standard clinical categories, thereby laying the groundwork for objective, standardized diagnoses.

[This page intentionally left blank]

Table of Contents

[This page intentionally left blank]

Problem Statement

Pitting edema is a symptom of the accumulation of intercellular fluid in tissue cells that results from an increase in interstitial fluid, characterized by swelling of tissues and formation of an indentation wherever pressure is applied to the skin. While early detection is critical because it indicates underlying heart, liver, or kidney issues, current diagnostic methods are subjective, relying solely on a clinician's visual assessment and grading of the skin indentation and rebound time. To address the lack of standardization, potential misclassification of severity, and delayed diagnosis, we designed a tonometer capable of applying a force and precisely measuring skin displacement and the normal force exerted by the skin on the device. This system would allow either healthcare professionals or researchers to collect data, helping them create a validated grading system. Future iterations of this system could also allow patients to measure the extent of their pitting edema, encouraging timely care-seeking behaviors that could support early diagnosis or better chronic disease management.

The overall goal of this project is to design a fully functional tonometer device that applies and measures force and displacement by pressing into the patient's tissue (typically on the forearm or calf), serving as a proof-of-concept design to provide clinicians with reliable, objective measurements to support the diagnosis and monitoring of pitting edema. To achieve this, we will design and implement subsystems for force sensing, displacement sensing, and actuation/pressurization.

A relatively long search for relevant studies and papers returned no devices that used similar methods to measure pitting edema. The most relevant paper we found was "Quantitative measurement of pitting edema with a novel edema ruler" [1], in which the team designed and 3D-printed a handheld tool to measure the depth of a pit created by manually applied pressure, which could then be used to help physicians in subjectively deciding an edema grade level for the patient. There has been some discussion of the lack of standardization in grading pitting edema [2], suggesting a common interest in a solution like the one we designed in our project. Similar circulatory issues can be detected with the peripheral arterial tonometry, a non-invasive test that assesses circulation by measuring changes in blood flow and arterial function [3]. This shows that using objective, sensor-based measurements has already improved the diagnosis of related issues, highlighting how our tonometer could help make edema assessments more consistent.

Purpose, Goals, & Objectives

The purpose of this project is to develop a prototype diagnostic tonometer device that applies force to the skin at various body locations to measure tissue displacement and objectively assess the severity of pitting edema. With this device, clinicians would be able to quantify the applied

force and the resulting tissue displacement, thereby standardizing the diagnostic method for edema.

This project supports the organizational objectives of creating a standardized diagnostic method to improve accuracy and consistency, and of creating a final wearable device ready for marketing to clinicians and, in the future, patients who want to self-assess at home. The business problem being addressed is the potential delay in diagnosis, which could lead to misclassification of disease severity and, in turn, increase care costs. This project has a high priority because this device can improve both clinical decision-making and self-monitoring for at-risk patients at home. In the long term, this device can improve chronic disease management and support preventive and remote monitoring.

The three main aspects of the project that are necessary to support the desired functionalities are (1) force sensing, (2) displacement sensing, and (3) pressure actuation. The force sensor records force data that may help researchers determine whether the amount of force applied is a variable that can guide methods for grading pitting edema. It also helps as a safety measure by creating a stopping point for the applied pressure, ensuring that reasonable pressure is applied so the patient does not get hurt. In future developments of this device, the force sensor will help create a feedback control system that applies the force needed to maintain constant tissue displacement, thereby helping determine the normal force exerted by the skin on the device. The displacement sensor measures the amount of tissue displacement created by the device's applied force, which is the main functionality of our device. The pressure actuation subsystem generates the pressure that induces indentation in the patient’s skin.

Dr. Chua’s team aims to develop a wearable device that precisely measures and categorizes pitting edema with minimal involvement from healthcare professionals. Before beginning our project, the device was at a Tech Readiness level of two (“Technology Conceptualized”) [4], with a timeline of 5 to 7 years before it could be implemented in a healthcare setting. Our project team aimed to demonstrate key elements in a laboratory environment that would indicate progression to a Tech Readiness level four (“Partial Scale Prototype & Modeling”) [4]. Our project is a prototype subsystem that will provide foundational data and establish a developmental framework for Dr. Chua’s team.

Background & Context

Pitting edema is usually checked using a pretty straightforward method: a doctor presses a finger into the patient’s skin, usually on the forearm or calf, and watches how deep the dent goes and how long it takes for the skin to bounce back. This “finger method” [5] is standard, but it is pretty subjective, meaning it depends heavily on the doctor's opinion of how bottomless the pit is and how quickly it rebounds. Because of this, different practitioners can end up grading it

inconsistently, which can slow down the diagnosis of serious issues like heart problems, kidney trouble, or liver disease.

To address this inconsistency, researchers have explored more precise methods. One notable innovation is the edema ruler [1], a small device made to measure the depth of the pit more accurately. While the ruler gives a specific number for the indentation's depth, it still relies on manual pressure and does not account for how quickly the skin rebounds or how evenly the pressure is applied. So, even though it is a step forward in accuracy compared to the finger method, it is not perfect for eliminating variability in assessment.

In practice, pitting edema is typically classified into four standard grades based on how deep the indentation is:

Table 1 - Pitting Edema Grade Scale [7]

Grade	Indentation Depth	Rebound Time
1+	< 2 mm	Immediately
2+	2 - 4 mm	< 15 seconds
3+	4 - 6 mm	< 60 seconds
4+	6 - 8 mm	$2 - 3$ minutes

While rebound time is important for identifying and classifying pitting, it was out of scope for this project. We hope that, with future updates using feedback-controlled actuation, we can add a rebound time to create a more rounded diagnostic tool.

By placing our work alongside existing diagnostic methods (such as the finger method and the edema ruler), the clinical grading standards, and the technical challenges of sensor development, this project shows both the need for and the potential of a standardized, quantitative tonometer for assessing pitting edema.

Success Criteria

The project will be a success if the following criteria are met or exceeded:

- The device can measure internal actuation displacement with an uncertainty of ±1 millimeter.
- The device can measure force at the end effector with an uncertainty of 10%.
- The device end-effector can detect contact with human skin within 0.5 seconds, with at least 1 newton of force applied.

- The device can extend and retract the end effector by at least 8mm at a frequency of at least 0.25 Hz.
- The device can record and share data that enables the classification of pitting edema into the four categories. The categories are defined by the pit depth: < 2 mm, 2-4mm, 4-6mm, and > 6 mm [7].
- The device complies with the standards listed below.

The constraint of measuring internal actuation displacement with an uncertainty of ±1 millimeter is most impactful to our device design, as it is our primary means of measuring pitting edema. In the most severe cases, pitting edema may produce depressions of around 8 millimeters, meaning that even small measurement errors could alter the assigned edema grade. Achieving ±1 millimeter uncertainty constrains the selection of sensors, mechanical tolerances of the pressure actuation subsystem, and the stiffness of the different materials used (silicone of the bellow, flexures of force capacitors, etc). It also influences the calibration process, necessitating the removal of noise or drift so that the measurements reflect close to true tissue indentation. This success criterion drove both mechanical and electrical design decisions and ultimately ensured the clinical meaningfulness of the device.

The constraint of measuring force with an uncertainty of 10% at the end effector is also meaningful to our device design, as it records the load applied to the skin, providing researchers with data that may show whether the applied force is a reliable parameter for guiding clinical grading pitting edema. It also functions as a safety mechanism by defining an upper limit on applied pressure, ensuring the device cannot exert excessive force that may cause patient discomfort or injury. This is one necessary part for future FDA approvals, as safety is a priority. In future iterations, accurate force measurement will be essential for implementing a closed-loop feedback controller that can modulate the actuation pressure to maintain a constant tissue displacement. This will allow the system to determine the normal force exerted by the skin against the device, another key parameter of interest. Because force interacts directly with the displacement-sensing and pressure-actuation subsystems, a 10% uncertainty constraint places strict requirements on sensor selection, mechanical design of the capacitor, and calibration, ensuring that the measured force reflects close to the true applied force and normal force rather than system noise or environmental noise.

The success criteria that the device should extend and retract the end effector by at least 8 millimeters at a minimum frequency of 0.25 Hz directly influences the design of the pressure-actuation subsystem. Because displacement is our primary measurement, the actuator must be capable of producing sufficient stroke length to replicate the full range of clinically relevant pitting-edema levels of depth. Meeting this displacement requirement ensures that we can reliably induce measurable pits across the full spectrum of edema severity. The frequency requirement of 0.25 Hz also constraints the performance of the actuator so that the system can

complete a full indentation-release cycle every four seconds. These constraints affect the selection of the actuation mechanism, the stiffness and response characteristics of the bellow, and the sizing and control strategy of the pneumatic subsystem. They also shape the decisions in making the overall mechanical design to ensure repeatable motion and minimal latency.

Technical Constraints

The accuracy of the force and displacement sensing portions of the device must remain within clinically acceptable tolerances, as the differences in displacement and force pushback from the skin are minute, and the degrees of pitting edema can differ by tiny increments. To provide meaningful diagnostic value, we must balance cost and sensor precision, and place strict requirements on sensor selection and calibration methods.

Another constraint during the prototype phase is size. To mimic current manual depression methods on the patient's skin, the device needs a pressure tip no larger than a thumb, or about 2 cm in diameter. The rest of the device needs to be compact enough to be made into a wearable device that securely fits on a person's limbs. Future iterations will need to consider shrinking the device to meet the size specifications required to make this into a wearable device.

Safety constraints should also be considered, as we want to ensure that safety restrictions are in place to prevent excessive pressure on the patient.

Standards

Our project will follow a set of standards to make sure the device is safe, reliable, and easy to integrate with other systems. On the regulatory side, we'll meet the FCC requirements under Title 47, Part 15 (Sections 15.23 and 15.5), which cover electronic emissions and interference. For the hardware, we'll use IEC 60320-1 for electrical connections and IPC-2221B for printed circuit board design (PCB). For communication, we'll rely on IEEE 1118.1-1990 for microcontroller control buses and the I2C protocol to handle data transfer between subsystems. Since this is a medical-focused project, we'll also reference ISO/IEEE 11073 standards to keep our device aligned with healthcare communication practices and patient safety.

1) *Generic Standard on Printed Board Design*, IPC-2221B, IPC, Bannockburn, IL, 2012. [Online]. Available: IPC_2221.pdf

IPC-2221B, Generic Standard on Printed Board Design, is an industry standard published by IPC that provides the design principles and requirements for printed circuit boards (PCBs). It covers material selection, conductor spacing, thermal management, mechanical layout, and electrical performance considerations. Its purpose is to ensure manufacturability and safety across PCB applications by establishing design rules that can be adapted to different technologies.

1) *Radio Frequency Devices,* Title 47 CFR Part 15, Federal Communications Commission, Washington, D.C., 2023. [Online]. Available: https://www.ecfr.gov/current/title-47/part-15

Under Title 47, Part 15 of the FCC rules, Section 15.23 allows individuals to build and operate low-power radio frequency devices for personal use without formal equipment authorization. Provided no more than five units are made, and they do not cause harmful interference. Section 15.5 sets out the operating conditions for all Part 15 devices. They must not cause harmful interference to licensed radio services, must accept any interference received, and must stop if ordered by the FCC.

2) *Universal Serial Bus Type-C Cable and Connector Specification,* Release 2.4, USB 3.0 Promoter Group, Oct. 2024. [Online]. Available: https://www.usb.org/document-library/usb-type-cr-cable-and-connector-specification-release-24

The USB Type-C Cable and Connector Specification Release 2.4 provides the newest framework for ensuring safety performance across devices that adopt the standard. This release refines definitions for cable assemblies, connector requirements, and extended power delivery. It introduces updated compliance requirements for USB4 Gen4 and liquid corrosion mitigation and alternate modes. For engineers and system designers, this serves as a reference for implementing Type-C technology in devices.

3) *IEEE Standard for Microcontroller System Bus*, IEEE Standard 1118.1-1990, 1990. [Online]. Available: https://ieeexplore.ieee.org/document/159173

The IEEE 1118.1-1990 standard defines the specifications for microcontroller control buses, providing a uniform method for communication between microcontrollers and peripheral devices. It establishes electrical, timing, and protocol requirements for data transfer, device interoperability, and control in embedded systems. By standardizing bus operations, IEEE 1118.1-1990 helps reduce design complexity, promotes hardware compatibility, and supports scalable system development.

4) *Solderability Tests for Component Leads, Terminations, Lugs, Terminals and Wires, Joint standard*, EIA/IPC/JEDEC J-STD-002E, IPC, EIA, and JEDEC, Nov. 2017. [Online]. Available:https://webstore.ansi.org/preview-pages/ipc/preview_j-std-002e.pdf?srsltid=AfmBOopS_s9edY3xJrSCdWhQsNor4nRz5zq07qOXc5j1KHITtFKT7D1X

The J-STD-002E standard provides a methodology for evaluating the solderability of component leads and wires used in electronic assemblies. It establishes visual criteria and force measurement tests. These procedures verify the components maintain acceptable solderability throughout storage and assembly. The standard helps suppliers and users ensure long-term reliability.

5) *Reference Designations for Electrical and Electronics Parts and Equipment*, ASME Y14.44-2008, The American Society of Mechanical Engineers, Nov. 21, 2008. [Online]. Available: https://www.intertekinform.com/preview/98393739772.pdf?sku=138813_SAIG_ASME_ASME_2631634&srsltid=AfmBOoqN_DQIZ4u7QUdkdc9FvU-_kXyi-eiCwLqGUh5Ni56hMhtX3eZU

This defines a uniform system for reference applied to electronic equipment. It specifies methods for unit numbering so that components are identifiable in documentation. Y14.44 reduces ambiguity in system layouts and supports manufacturing teams.

6) IPC-A-610E: Acceptability of Electronic Assemblies, IPC – Association Connecting Electronics Industries, Apr. 2010. [Online]. Available: https://datasheet.datasheetarchive.com/originals/crawler/acdi.com/4fa15157e5b81fef1873e725a900d3e8.pdf

The standard provides criteria for the inspection and quality evaluation of electronic assemblies. It establishes classifications for assemblies. Class 1: general electronic products, Class 2: dedicated service, and Class 3: high-performance.

Approach & Design Methodology

Our approach uses three main subsystems: Force sensing, displacement sensing, and pressure actuation. We chose this path because it strikes a balance among accuracy, safety, and practicality, while also building on methods that are more reliable than current clinical evaluations.

We felt this was the best direction compared to existing options, such as simple mechanical tonometers, which aren't very accurate and depend heavily on the clinician. Our approach enables more objective and repeatable results, setting the stage for future improvements to wearable devices.

Force Sensing

While working on our prototype, we ran into familiar measurement issues. At first, we considered using a standard resistive force sensor, but they are often inaccurate, prone to drift, and challenging to customize. To tackle these problems, we decided to design and build our own capacitive force sensor. Since we were on a tight budget, we used two copper pennies from before 1982 as the capacitor plates. While this worked, it came with its own set of challenges: pennies are less conductive than aluminum and are more affected by environmental noise. With a larger budget, we would have substituted the pennies for slices of aluminum rods for the capacitor plates to improve conductivity and reduce sensitivity to noise.

We designed our capacitor using two isolated copper plates. These have a capacitance between them that can be measured using a capacitive-to-digital chip. The plates are mounted on a flexure that compresses when force is applied. These plates were sized appropriately and fixed at a 1.5 mm distance to ensure the reading of a maximum capacitance of 15 pF when applying a maximum force of 10 N. This was done to ensure that the applied force remained within the FDC1004's range, a four-channel capacitive-to-digital converter.

Calibration was another big hurdle. The capacitive sensor was picking up significant external noise, so we implemented a digital low-pass filter, or specifically a first-order Butterworth low-pass filter, to smooth the signal and remove noise.

This filter is defined by its discrete-time transfer function $H[z] = \frac{\omega_0}{\frac{2}{T_s}[\frac{1-z^{-1}}{1+z^{-1}}] + \omega_0}$, where ω_0 is the cutoff frequency and T_s is the sampling period. And the corresponding difference equation we used to implement this filter is $y[k] = (\frac{2-\omega_0 T_s}{2+\omega_0 Ts})y[k-1] + \frac{\omega_0 T_s}{2+\omega_0 Ts}x[k] + \frac{\omega_0 T_s}{2+\omega_0 Ts}x[k-1]$.

Even with filtering, some readings were too weak to be useful, so we added an amplifier to boost the signal into a measurable range. While calibrating, we also realized that the flexure holding the pennies was flawed in that the flexure would not rebound fully over time, causing drift in our capacitance measurements. These steps were essential for meeting our accuracy goals, but they really highlight how tough it can be to build reliable biomedical sensors when resources are limited.

Displacement Sensing

To measure skin response, we used a photodiode displacement sensor. This sensor will help us track how far the skin is displaced. This works by measuring the internal displacement of the bellow through emitting and detecting infrared light. By measuring the current generated by the photodiode, we can determine how close the opposite side of the bellow is to the sensor. We chose this method due to its low cost, precision, and ease of integration compared to more bulky or less accurate alternatives.

Pressure Actuation

For the actuation subsystem, we developed a pneumatic bellow to apply controlled pressure in the y-direction. Our first version was inspired by a Soft Robotics project that focused on pneumatic actuators, which we used as a guide for designing the mold and its shape [6]. We made a two-piece mold for the bellow, keeping three main things in mind: wall thickness, folding angle, and fold shape.

For wall thickness, we went with 3 mm after reviewing a research paper on soft-bellow actuators [7]. At 50 kPa, this thickness yielded the best deformation, with a displacement of 14.58 mm. In contrast, a six mm-thick option only provided 5.49 mm of movement [7]. While the original actuator was for a different purpose, the design and pressure factors still worked for what we were trying to do.

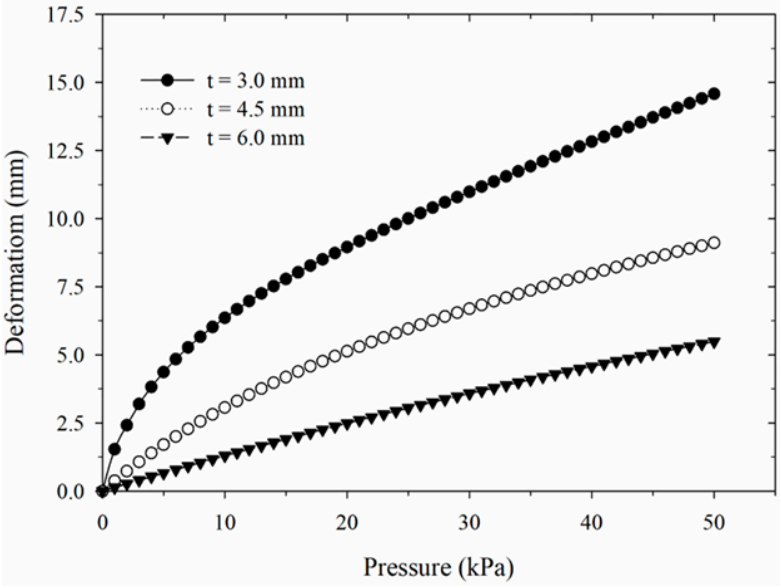

Figure 1: Simulation result of deformation response under 50 kPa pressure with wall thickness of 3mm [7]

We chose a folding angle of 30° based on the techniques described in the paper on soft bellow actuators and on Dr. Chua's previous work with mechanical bellow designs [8]. For the fold shapes, we kept it simple with triangular designs, following the guidelines from the Soft Robotics project [7].

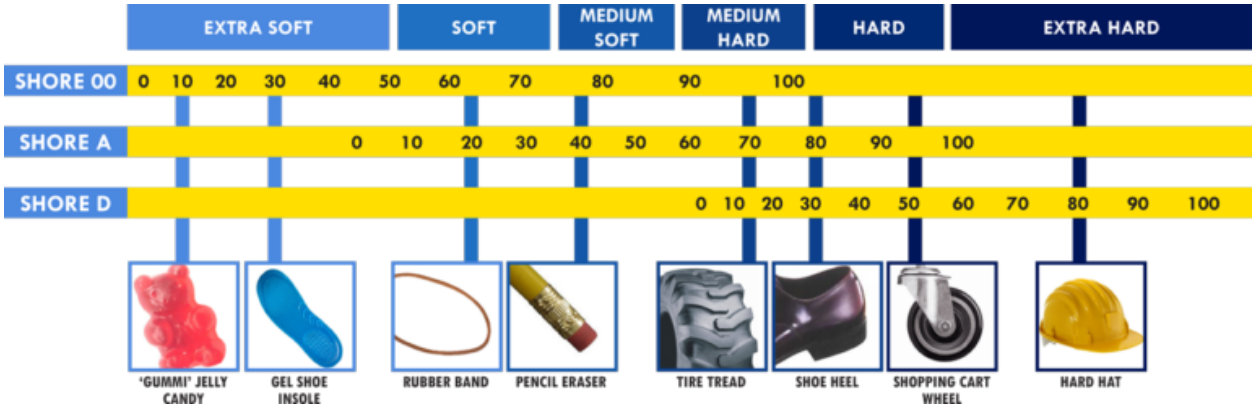

Figure 2: Silicon Shore Hardness Scales [9]

For the materials, we cast the bellow in Dragon Skin 20A silicone rubber. This was a good choice because it is as flexible as a rubber band, and we thought it would let the bellow expand up to 12 mm, which was our goal. We also used epoxy glue made for silicone to stick the two halves together since we cast it in two parts.

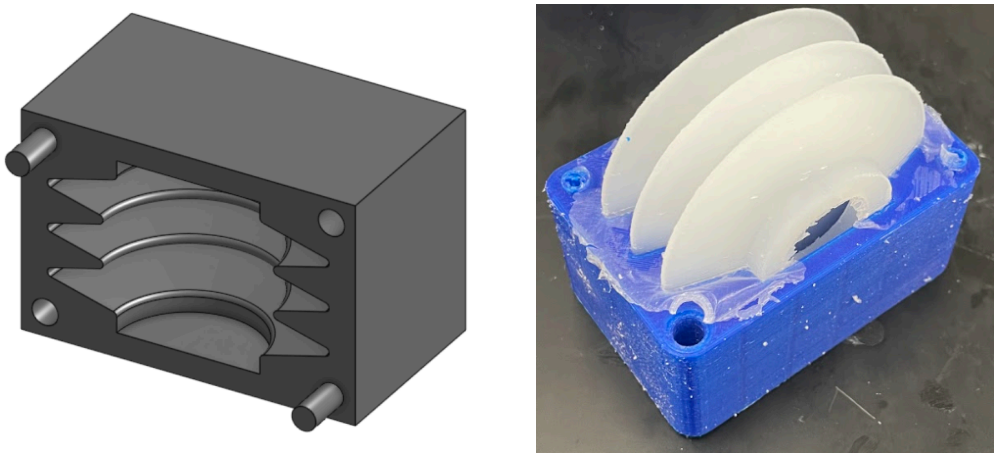

Figure 3 - Bellow Mold and Cast

Testing it with a syringe showed that our first design did not quite reach the target of 12 mm, expanding only to 8 mm. To fix that, we created a second design with some changes: we added a fourth fold to increase the expansion area, reduced the wall thickness from 3 mm to 2.5 mm for greater flexibility, and switched the material from Dragon Skin 20A to Silicone Shore 0030 for even greater compliance. These tweaks improved the actuator's performance and helped it get closer to meeting our displacement goals.

Physical Device

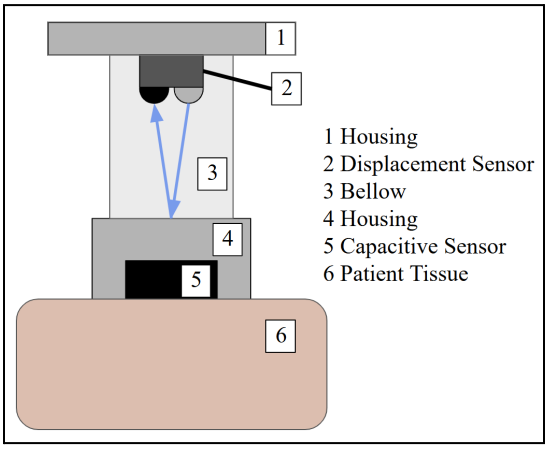

Figure 4: Hardware Design Overview

Figure 4 shows the design overview and how the device is supposed to work. As the bellow is inflated, the distance between the housings will increase, and this will be read using an infrared emitter and detector sensor circuit. The force of the patient's tissue against the device will be measured using the capacitive sensor. This way, we can determine whether we are in contact with the patient, whether the tissue is responding in a way consistent with edema, and how deep the tissue has been displaced.

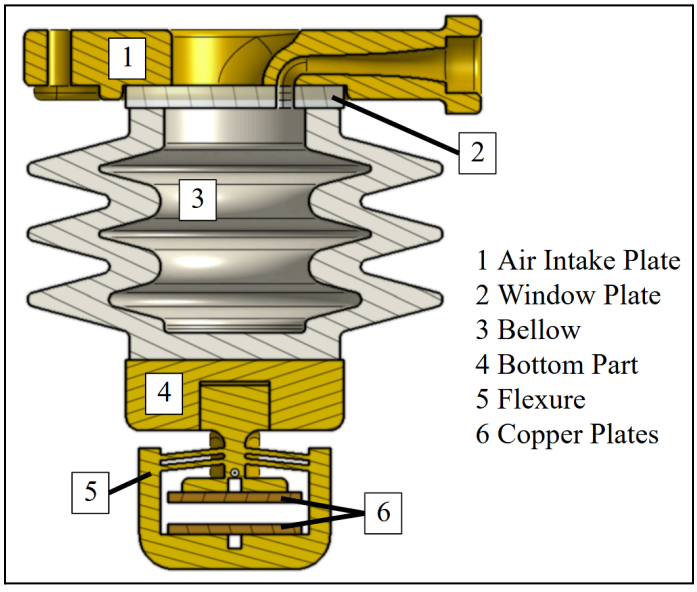

Figure 5: Physical Computer-Aided Design

The physical design consists mainly of the components listed above. This is in addition to the printed circuit board mounted on the air intake plate, several wires, and the air intake hose. This design was created in Onshape, a computer-aided design (CAD) software.

Circuit Design

Schematics for the displacement sensor, capacitance sensor, and ESP32 pinout and connections were all designed in KiCAD, a circuit design software. Then, these schematics were combined and translated into a printed circuit board layout in KiCAD. The printed circuit board was designed to implement shielding for our capacitive sensor, mitigate environmental noise with two-layer ground fills, and parallel traces to reduce crosstalk.

Alternative Designs

Both the physical and circuit designs had multiple iterations. Shown below are some iterations for each component.

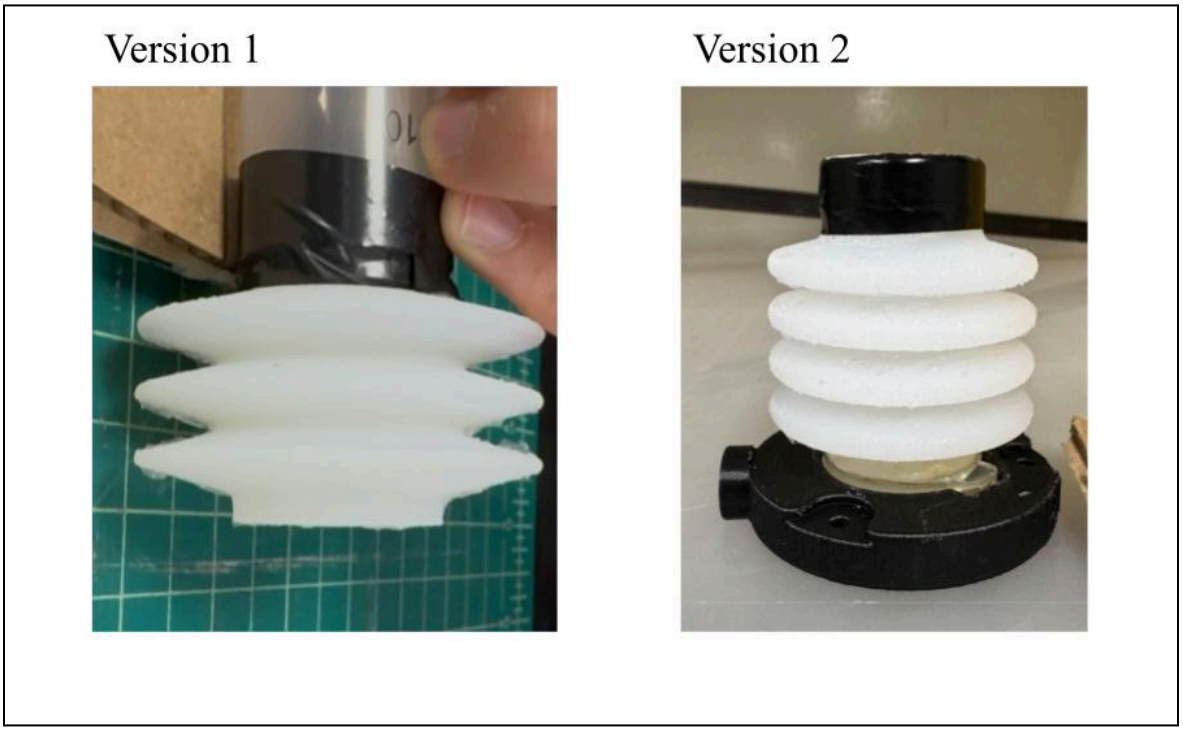

Figure 6: Bellow Iterations

Bellow version 1 did not have adequate extension when inflated. For this reason, and to create a thicker wall for better adhesion to the top and bottom fixtures, version 2 was created.

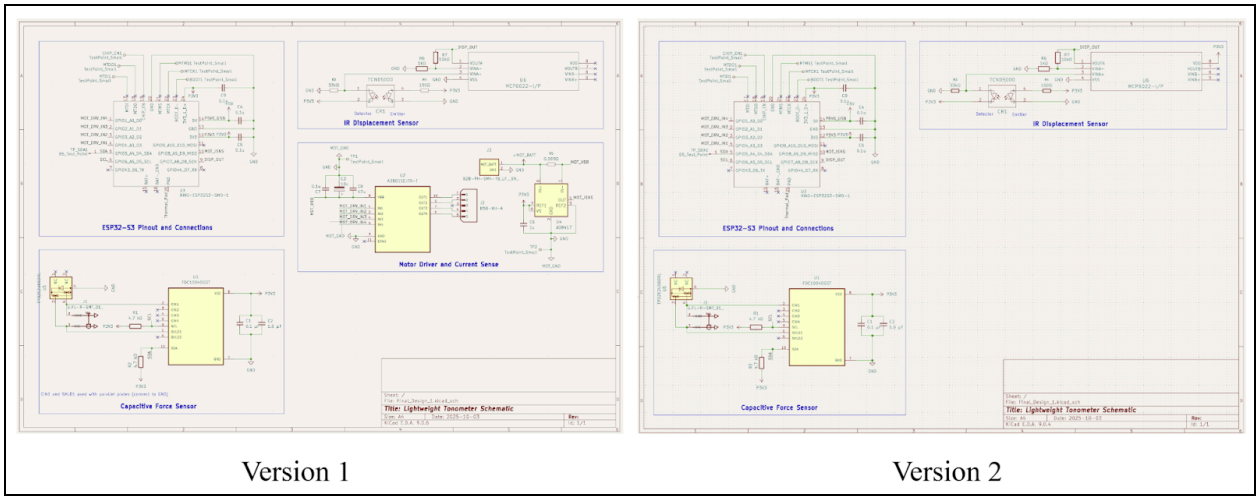

Figure 7: Schematic Iterations

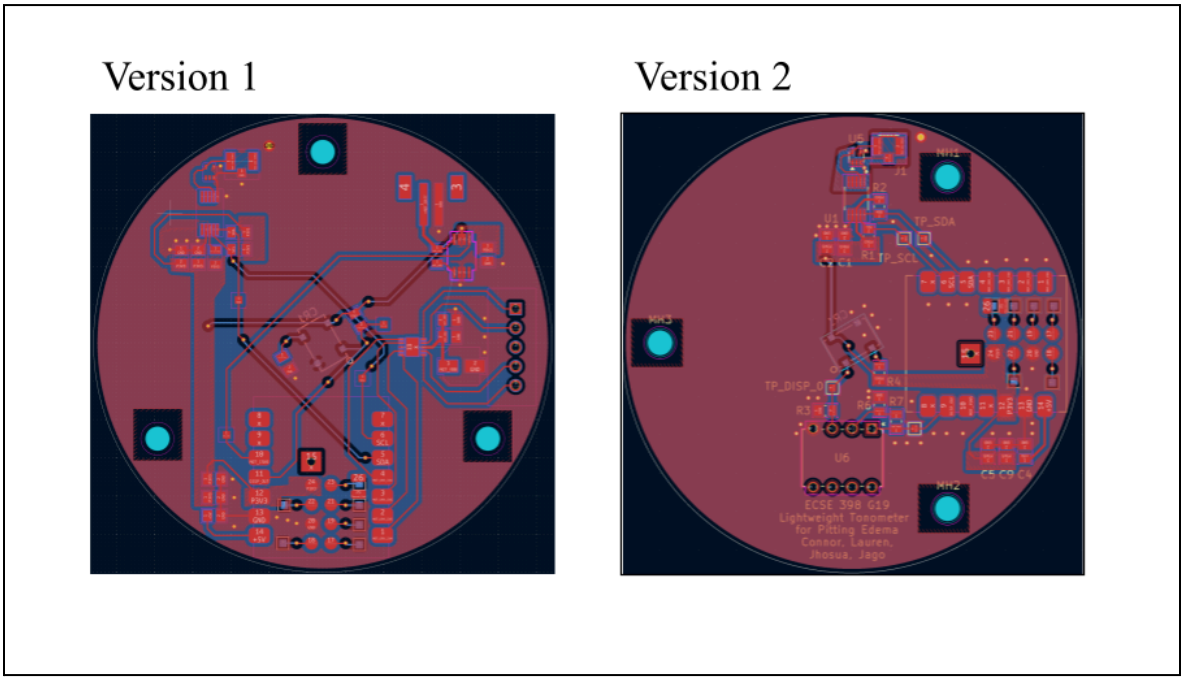

Figure 7: PCB Iterations

After testing our first PCB, we determined that the displacement sensor did not vary enough to provide accurate data and was highly susceptible to external noise. After troubleshooting and experimentation, we found a solution, implemented it in our second schematic version, and then updated the PCB design. In addition, we removed the current-sense feature and motor-driver connectors, which were used when the project had a broader scope. We also widened the driving-voltage traces and added a through-hole for an operational amplifier to increase gain in the displacement sensor's output. As a precaution, we also redesigned the capacitance force sensor circuitry to improve I2C connectivity by shortening the SDA and SCL traces, making

them as parallel as possible, and ensuring there were no breaks in the ground plane beneath the traces and pins.

By combining these subsystems, we designed a proof-of-concept device that integrates force sensing, displacement measurement, and pneumatic actuation into a single system.

Verification & Results

Our first criterion was to ensure that our device measures internal actuation displacement with an uncertainty of ±1 millimeter. This was established using the TCND5000 IR sensor, implementing a first-order, digital low-pass Butterworth filter and a moving average function to reduce noise, situating our IR sensor perpendicular to a wall, and using a caliper to corroborate distances to voltage readings with the sensor. As a result, we decided to set the cutoff frequency 10 Hz, the sampling period 0.01 seconds per sample, and averaged over 50 samples. From the difference equation and these values, we obtained coefficients $a = 0.7285$ and $b = 0.1358$. In doing so, we uncovered a non-linear relationship between these two readings and obtained a fourth-order polynomial function that fit our data. From this fit, we obtained a minimum standard error of 0.0 mm, a maximum standard error of 0.7 mm, and an average standard error of 0.3167 mm, which met our 1 mm uncertainty criterion.

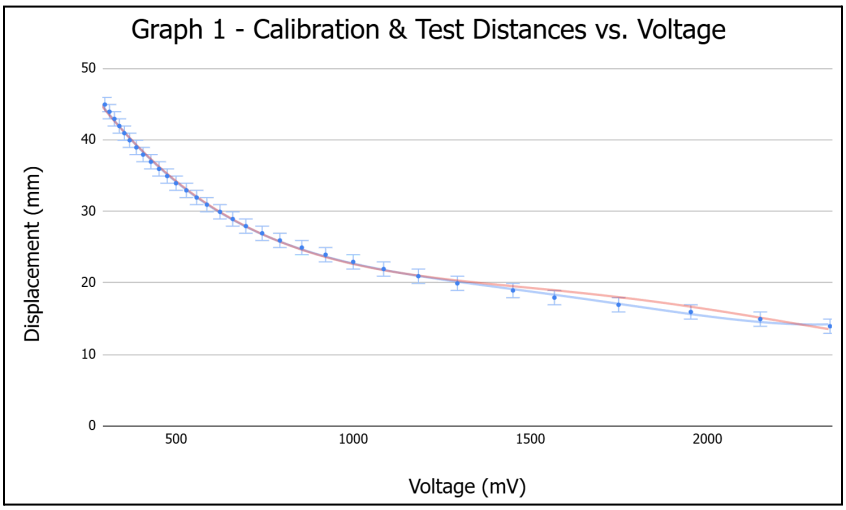

Figure 8: Graph of Calibration (Blue) and Test (Red) Distances with Voltage

Our second criterion was to ensure the device measures force with the end effector within 10% uncertainty. Under the right conditions, we were able to obtain measurements with an uncertainty of 10%. This was done by using two copper plates mounted within a flexure, with calibration weights placed directly on top of the flexure, which was mounted perpendicular to the surface. However, environmental interference and minor flaws in our flexure's mechanical design

hindered our ability to corroborate capacitance readings with the applied weight consistently. We also implemented the same first-order, low-pass digital Butterworth filter, combined with a moving average, to reduce interference and noise. Although we were able to reduce most of the noise, the sensor's sensitivity still caused environmental interference in our readings. This could be improved by incorporating additional shielding, adding a dielectric material, fully enclosing the capacitors, and creating a more robust flexure design to reduce environmental noise as much as possible.

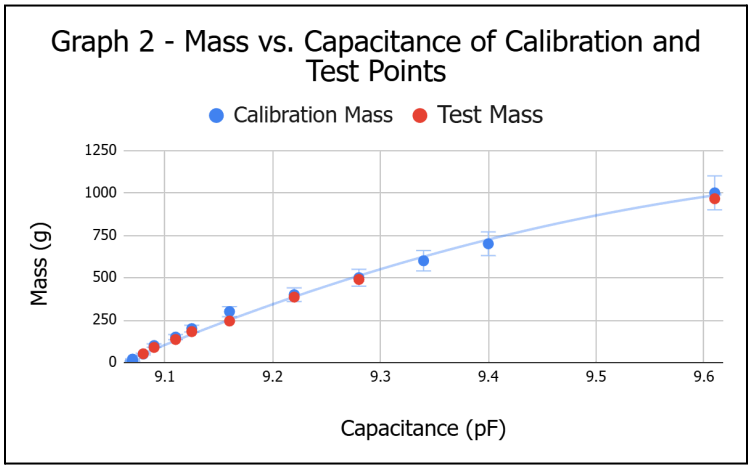

Figure 9: Graph of Calibration and Test Masses with Capacitance

Our third criterion was to ensure the device's end effector could detect contact with human skin within 0.5 seconds with at least 1 N of force applied. Using our calibration weights and I2C communication with our ESP32, we consistently obtained force measurements from 1 N to 10 N in under 0.5 seconds. Thus, we met this criterion.

Our fourth criterion was to ensure that the device extends and retracts the end effector by at least 8mm at a frequency of at least 0.25 Hz. This was met, as we obtained about 35 mm of extension and retraction at about 0.4 Hz. This was measured by recording a video of the bellow being extended and retracted next to a ruler, with a timer in the background, so that the extension amount and the frequency of each extension and retraction cycle could be determined from the video playback.

Our fifth criterion was to ensure the device records and shares accurate data to classify pitting edema into the four categories or specified grade levels. To do so, we relied on the TCND5000, our IR displacement sensor. From corroborating measured displacement and the actual displacement associated with the specified grade level, we met this criterion. Figure 10 below depicts how our measurements align with the categorized grade levels, indicating a high success rate. The reason our third measurement is not correct is that it falls between grades 1 and 2 and differs by approximately 0.1 mm. However, this was not the case for other borderlines.

Actual Displacement (mm)	Grade Level	Measured Displacement (mm)	Categorized Grade Level	Correct
1	1	1.18	1	Yes
1.5	1	1.44	1	Yes
2	2	1.88	1	No
2.5	2	2.4	2	Yes
3	2	3.13	2	Yes
3.5	2	3.65	2	Yes
4	3	4.02	3	Yes
4.5	3	4.73	3	Yes
5	3	5.18	3	Yes
5.5	3	5.7	3	Yes
6	4	6.1	4	Yes
6.5	4	6.48	4	Yes
7	4	6.95	4	Yes
7.5	4	7.35	4	Yes

Figure 10: Table of Actual Displacement Measurements and Categorized Grade Level

Lastly, our sixth criterion was to meet our necessary standards. From the completion of this project, we fully met each standard. That is, FCC requirements under Title 47, Part 15 (Sections 15.23 and 15.5), IEC 60320-1, IPC-2221B, IEEE 1118.1-1990, ISO/IEEE 11073, J-STD-002E, and IPC-A-610E.

Project Management

We used a Gantt chart to assign and track tasks throughout the project. The Gantt chart below shows task categories, task numbers with their respective milestones, task predecessors, specific task leaders and members, and the duration of each task throughout the project timeline. Figure 11 shows a Gantt chart. Additionally, Dr. Chua assigned us a $100 budget for this project.

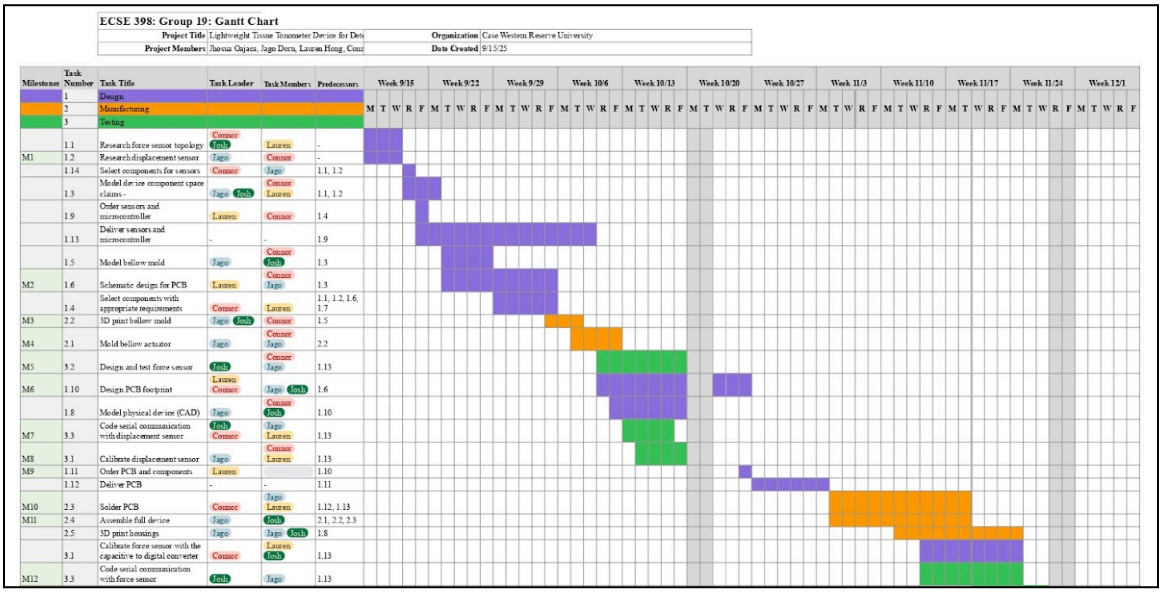

Figure 11: Gantt Chart for Project Management

Relevant Courses

Table 1: Relevant Courses with Listed Group Members and Description of Course Relevance

Course	Taken By	Description
ENGR 210	Jago Dorn, Jhosua Oajaca, Lauren Hong, Connor Kissack	● Circuit analysis ● Electrical power ● Operational Amplifiers
ECSE 245	Jago Dorn, Jhosua Oajaca, Connor Kissack	● Additional complex circuit analysis with diodes ● Spice software
ECSE 395	Jhosua Oajaca	● Project management ● Identifying technical constraints
ECSE 326	Jago Dorn	● Capacitive and optical design ● Noise filtering ● Analog to digital signal conversion
ECSE 313 / EBME 309	Jago Dorn, Jhosua Oajaca, Connor Kissack / Lauren Hong	● Digital Butterworth filter implementation ● Laplace transforms ● Frequency filtering
ECSE 344	Connor Kissack	● Implementation and design of real-world circuits under physical constraints
ECSE 488	Lauren Hong	● Arduino IDE ● Embedded systems design ● IR sensors ● Project management
ECSE 309	Jhosua Oajaca, Connor Kissack, Lauren Hong	● Understanding and physical properties of capacitors

Appendix A - Arduino Code for Calibration of FDC1004 and TCND5000

```
/********** Combined FDC1004 + TCND5000 **********/
#include <Wire.h>
#include <FDC1004.h>

/* ---------------- FDC1004 Setup ---------------- */
const int SDA_PIN = SDA;  // GPIO5 = SDA on XIAO ESP32S3
const int SCL_PIN = SCL;  // GPIO6 = SCL on XIAO ESP32S3

// Digital Low Pass Butterworth Filter for FDC
float yk1 = 0; // y[k-1]
float xk1 = 0; // x[k-1]
const float a = 0.72848950367272; // cutoff = 10 Hz
const float b = 0.13575752481636; // sampling = 100 S/s
FDC1004 fdc(FDC1004_100HZ);

/* ---------------- TCND5000 Setup ---------------- */
const int DISP_OUT = A8;

// Low pass filter parameters
float r = 30000;
float c = 0.000000483;
float sample_period = 0.01;
float cutOff_frequency = 1 / (2 * PI * r * c);
float sampling_rate = 1 / sample_period;
float smoothing_factor = expf(-2 * PI * cutOff_frequency / sampling_rate);
float filteredValue = 0.0;

/* ---------------- Arduino Setup ---------------- */
void setup() {
```

```
  Serial.begin(115200);
  // Initialize I2C for FDC1004
  Wire.begin(SDA_PIN, SCL_PIN);
  Wire.setClock(100000); // 100 kHz I2C
  delay(50);
  Serial.println("FDC1004 ready (Wire initialized).");

  // Initialize TCND5000 pin
  pinMode(DISP_OUT, INPUT);
  Serial.println("TCND5000 ready.");
}

/* ---------------- Arduino Loop ---------------- */
void loop() {
  /*********** FDC1004 Reading ***********/
  float c_fF = fdc.getCapacitance(0); // read CIN1
  float pf = c_fF / 1000.0;           // convert to pF

  // Butterworth filter
  float yk_c = a * yk1 + b * pf + b * xk1;

  Serial.print("FDC1004: ");
  Serial.println(yk_c, 2);

  xk1 = pf;
  yk1 = yk_c;

  /*********** TCND5000 Reading ***********/
  int samples = 50;
  float total = 0.0;
```

```
  for (int i = 0; i < samples; i++) {
    float raw = analogRead(DISP_OUT);
    filteredValue = (1.0f - smoothing_factor) * raw + smoothing_factor *
filteredValue;
    total += filteredValue;
    delayMicroseconds(100);
  }
  float average = total / samples;
  float voltage_mV = (average / 4095.0) * 3300.0;
  double displacement = 70 - 0.112 * voltage_mV + 1.01e-4 * voltage_mV *
voltage_mV - 4.22e-8 * voltage_mV * voltage_mV * voltage_mV + 6.54e-12 *
voltage_mV * voltage_mV * voltage_mV * voltage_mV;


  Serial.print("TCND5000 displacement = ");
  Serial.println(displacement);
  if (displacement < 2) {
    Serial.println("Grade level: 1");
  } else if (displacement < 4) {
    Serial.println("Grade level: 2");
  } else if (displacement < 6) {
    Serial.println("Grade level: 3");
  } else if (displacement < 8) {
    Serial.println("Grade level: 4");
  }
  // Example combined CSV-style output for plotting
  Serial.print("PlotData: ");
  Serial.print(yk_c, 2);      // capacitance (pF)
  Serial.print(", ");
  Serial.println(voltage_mV); // displacement voltage (mV)
  delay(10); // small delay before next loop
}
```

Appendix B: Circuit Schematics

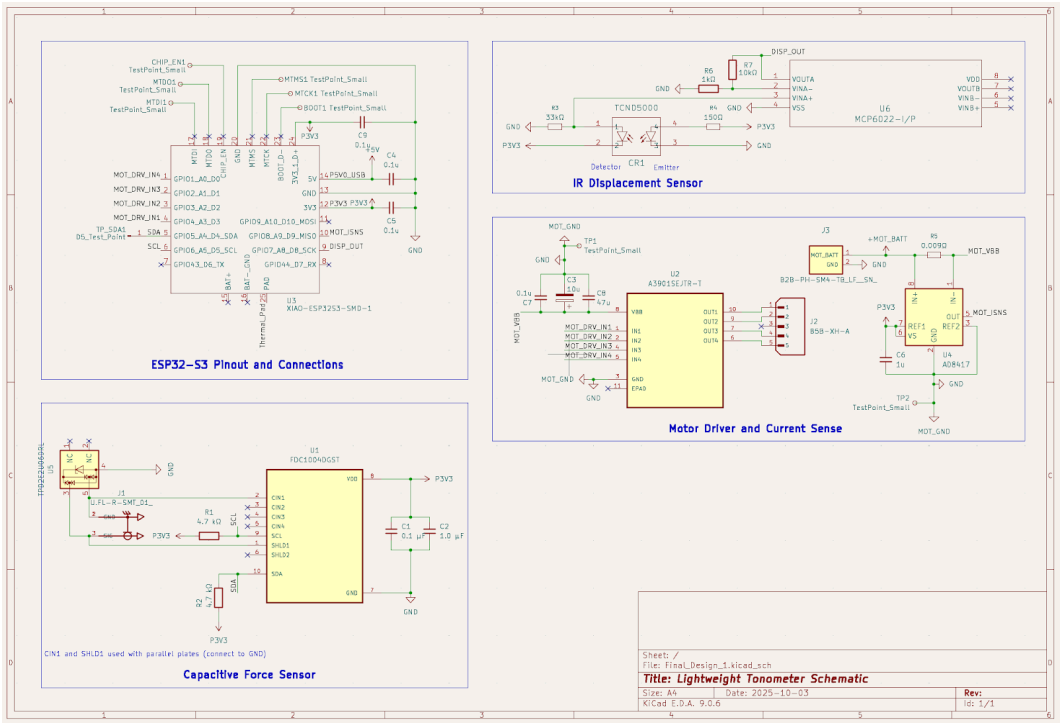

Figure 12 Version 1 Schematics

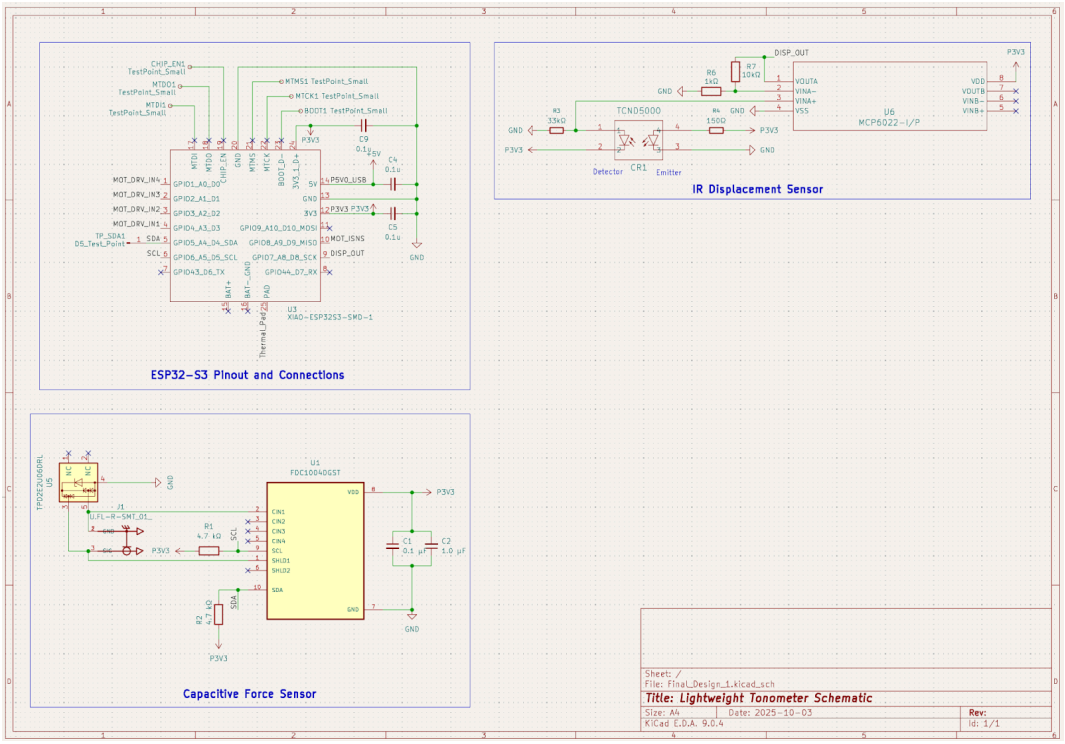

Figure 13: Version 2 Schematics

References

[1] Calzon, Maysen E, J. Blebea, and C. Pittman, “Quantitative measurement of pitting edema with a novel edema ruler,” Journal of Vascular Surgery Cases, Innovations and Techniques, vol. 10, no. 1, 2024, doi: https://doi.org/10.1016/j.jvscit.2023.101373. Available: https://doi.org/10.1016/j.jvscit.2023.101373.

[2] Mayo Clinic, “Edema - symptoms and causes,” Mayo Clinic, Jul. 28, 2023. Available: https://www.mayoclinic.org/diseases-conditions/

[3] “Peripheral Arterial Tonometry: Non-Invasive Test for Vascular Health - The Kingsley Clinic,” *The Kingsley Clinic*, 2025. https://thekingsleyclinic.com/resources/peripheral-arterial-tonometry-non-invasive-test-for-vascular-health/ (accessed Dec. 03, 2025).

[4] K. Wolf-Cloud, “What are Technology Readiness Levels, and where is Wind Harvest in the process towards full commercialization of the first utility-scale H-type turbine?,” *Wind Harvest*, Dec. 01, 2021. https://windharvest.com/blog/faq-items/what-are-technology-readiness-levels-and-where-is-wind-harvest-in-the-process/

[5] Cleveland Clinic, “Edema: Causes, Symptoms & Treatment,” *Cleveland Clinic*, May 17, 2022. https://my.clevelandclinic.org/health/diseases/12564-edema (accessed Dec. 03, 2025).

[6] T. Bieze, F. Largillière, and S. Hage Chehade, “FeTCh Mark 1 Manipulator | Soft Robotics Toolkit,” *Soft Robotics Toolkit*, 2015. https://softroboticstoolkit.com/fetch (accessed Dec. 03, 2025).

[7] Jutamanee Auysakul, Apidet Booranawong, Nitipan Vittayaphadung, and Pruittikorn Smithmaitrie, “An Optimized Design of the Soft Bellow Actuator Based on the Box–Behnken Response Surface Design,” *Actuators*, vol. 12, no. 7, pp. 300–300, Jul. 2023, doi: https://doi.org/10.3390/act12070300.

[8] J. Su, K. Zuo, and Z. Chua, “Three Degree-of-Freedom Soft Continuum Kinesthetic Haptic Display for Telemanipulation Via Sensory Substitution at the Finger,” Research Gate, Sep. 17.

[9] Zeke and Zeke, “Industrial Silicone Hardness Guide: Choosing the Right Shore A for Your Application,” *Custom Silicone Molding*, Jul. 24, 2025. https://www.newtopcustomsilicone.com/industrial-silicone-hardness-guide-choosing-the-right-shore-a-for-your-application/